

Blazar halos as probe for extragalactic magnetic fields and maximal acceleration energy

K. Dolag,¹ M. Kachelrieß,² S. Ostapchenko,^{2,3} and R. Tomàs⁴

¹*Max-Planck-Institut für Astrophysik, Garching, Germany*

²*Institutt for fysikk, NTNU, Trondheim, Norway*

³*D. V. Skobeltsyn Institute of Nuclear Physics, Moscow State University, Russia*

⁴*II. Institut für theoretische Physik, Universität Hamburg, Germany*

(Dated: March 12, 2009)

High energy photons from blazars interact within tens of kpc with the extragalactic photon background, initiating electromagnetic pair cascades. The charged component of such cascades is deflected by extragalactic magnetic fields (EGMF), leading to halos even around initially point-like sources. We calculate the intensity profile of the resulting secondary high-energy photons for different assumptions on the initial source spectrum and the strength of the EGMF, employing also fields found earlier in a constrained simulation of structure formation including MHD processes. We find that the observation of halos around blazars like Mrk 180 probes an interesting range of EGMF strengths. Blazar halos test also if the photon energy spectrum at the source extends beyond ~ 100 TeV and how anisotropic this high energy component is emitted.

PACS numbers: 98.70.Sa, 95.85.Pw, 98.54.Cm, 98.62.En

I. INTRODUCTION

Observations of photons with energies up to tens of TeV, mainly by imaging air Cherenkov telescopes (IACT), have opened in the last decade a new window on the non-thermal side of the Universe [1]. One of the main aims of these observations is the identification of the sources of cosmic rays and their acceleration mechanism. Observations of very high energy photons can however provide information on many more areas of astrophysics, as e.g. the amount of extragalactic background light (EBL) and the strength of extragalactic magnetic fields (EGMF).

The tight relationship between the EBL, the strength of EGMFs and the horizon of high energy photons is well-known: Photons with energy above the pair creation threshold, $E_{\text{th}} \sim 30$ TeV, can interact with background photons, initiating electromagnetic pair cascades [2]. The charged component of such cascades is in turn deflected by magnetic fields, first by fields in the cluster surrounding the source [3] and then by EGMFs [4]. If the EGMF is not extremely weak, $B \lesssim 10^{-16}$ G, secondary photons are deflected outside a point-like source and thus the observed point-like photon flux $I(E)$ consists only of the surviving primary photons, $I(E) = \exp[-\tau_{\gamma\gamma}(E)]I_0$, with $\tau_{\gamma\gamma}$ as the depth for pair production. If the EGMF is of order $(10^{-11}-10^{-12})$ G in a large volume fraction, the deflections and thus the halo extension may be sufficiently small that an observation by current or next generation IACTs may be feasible [4].

We focus in this work on the effect of EGMFs on electromagnetic cascades, providing detailed predictions for the expected intensity $I(E, \vartheta)$ of the halo produced by cascades as function of the observed energy E and the angular distance ϑ to the source. Since the EGMF is highly structured and the Milky Way is contained in the supagalactic plane, the magnetic field along the line-of-

sight to different blazars, and thus also their halos, will vary significantly, even if they would be at the same distance and would have the same source energy spectrum. It is therefore crucial to use an EGMF model that describes at least qualitative correctly the location of voids and filaments. Since deflections close to the observer are most important, it is sufficient to account for the EGMF structure of the local universe. For our predictions of the expected halo intensity $I(E, \vartheta)$ around selected blazars we use therefore EGMF models calculated in Ref. [5] that are based on a constrained simulation of the large-scale structure within ≈ 115 Mpc.

Our results confirm the estimate of Ref. [4] that blazar halos are detectable, if EGMFs are as weak as found in the simulations of Ref. [5]. Thus blazar halos may provide valuable information about the strength of EGMFs in a range where other tools like Faraday rotation measurements can give only upper limits. Moreover, our detailed predictions for the expected intensity $I(E, \vartheta)$ of the halo produced by the electromagnetic cascade allow one to disentangle the contributions from secondaries generated close to the source, as suggested in Ref. [3], and during propagation in the EGMF. The intensity of the halo is also sensitive to the total luminosity of the source above ~ 100 TeV and to the opening angle ϑ of the cone in which most of this high energy radiation is emitted.

We find that the measured energy spectrum of most blazars detected with IACTs may be described by a broken power-law that is steeper in the measured energy range (100 GeV–few TeV) than usually assumed, if one adds a softer high energy component. This additional high-energy component is absent both in Synchrotron Self-Compton and Inverse Compton models for blazars [6], but may be caused by hadrons [7]. In most hadronic models, e.g. acceleration close to the core in electromagnetic fields or in hot spots, the bulk of radiation is, although emitted anisotropically, extends over a

cone with opening angles $\vartheta \gtrsim 10^\circ$. For such conditions, we found that the halo is not strongly suppressed. Thus the observation of blazar halos would be an indication for an extension of the source photon spectrum beyond 100 TeV that is not strongly beamed and thus also evidence for the acceleration of hadrons in blazars.

This article is structured as follows: We start in Sec. II with a brief description of our Monte Carlo (MC) scheme. Then we study in Sec. III a toy model that allows us to exhibit clearly the dependence of the halo properties on external parameters as the strength of the EGMF, the source photon energy spectrum and the amount of beaming. In Sec. IV, we use magnetic fields from Ref. [5] along the line-of-sight towards four selected blazars and calculate their halos, choosing the source energy spectrum such that the observed photon spectra at low energies are reproduced. Finally, we summarize in Sec. V.

II. MONTE CARLO SCHEME

We choose to describe the propagation of the electromagnetic (e/m) cascade in the extragalactic space using a MC method. Starting from an initial photon emitted by the source, we trace the development of the cascade taking into account e^+e^- pair production by photons and inverse Compton scattering (ICS) of electrons due to their interactions with photons from the radio, infra-red, and the microwave background as well as synchrotron energy losses of electrons. For the spectral densities of the backgrounds we use the “Best-Fit06” model from Ref. [8] for the EBL and Ref. [9] for the radio background.

Since we are interested in gamma-rays arriving to the observer with small angular deflections, we can use an essentially one-dimensional picture for the propagation of the e/m cascade. A typical propagation pattern is sketched in Fig. 1. The initial photon is emitted by the

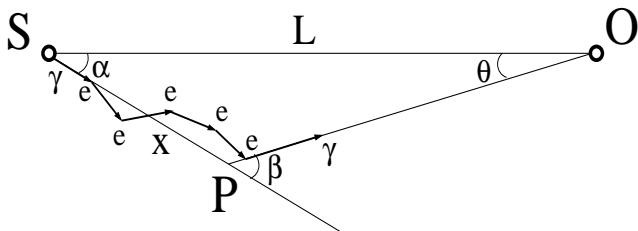


FIG. 1: Schematic view of the electromagnetic cascade in extragalactic space.

source S with the angle α with respect to the direction to the observer O . Due to interactions of both the initial photon and of secondary leptons, an e/m cascade develops over the distance x , until at point P the final photon is produced. This photon arrives to the observer under the angle ϑ with respect to the direction to the source, while its wave-vector forms the angle β with respect to the initial photon direction. The three angles ϑ , α , and

β are related by

$$\alpha = \beta - \vartheta, \quad (1)$$

$$\sin \vartheta = \frac{x}{L} \sin \beta. \quad (2)$$

For small ϑ we are interested in, we have

$$\vartheta \simeq \frac{x \sin \beta}{L - x \cos \beta}. \quad (3)$$

We calculate the average scattering angle β within the small angle approximation as

$$\beta = \sqrt{\langle \beta^2 \rangle} = \sqrt{\sum_i \beta_i^2}, \quad (4)$$

with β_i^2 as angular deflection of the electron i during the cascade development. The deflection angle in a regular magnetic field is

$$\beta_i \simeq \frac{d}{R_L} \simeq 0.52^\circ \left(\frac{p_\perp}{10^{20} \text{ eV}} \right)^{-1} \left(\frac{d}{1 \text{ kpc}} \right) \left(\frac{B}{\mu\text{G}} \right) \quad (5)$$

for a particle with momentum p_\perp perpendicular to B propagating the distance d .

As it can be read off from Eq. (3), the effect of deflections β at large distances from the observer is suppressed by the ratio x/L compared to those close by. Hence an important contribution to the halo at small ϑ are final photons produced at $x \ll L$, and passing the remained distance $L - x$ without interactions. A competing although less important contribution comes from photons with small scattering angle β . In particular, the latter is somewhat enhanced in the case of a structured EGMF: Filaments of the EGMF may be crossed by intermediate photons in the e/m cascade, while intermediate electrons propagate in the voids. As a result, the strength and the structure of the magnetic field close to the observer is more important than the “average” field.

III. PARAMETER DEPENDENCE OF THE HALO IN A TOY MODEL

The intensity and the extension of the halo around a blazar caused by the deflection of e^+e^- pairs in the electromagnetic cascade depends mainly on the strength and the structure of the EGMF, the spectral shape of the source spectrum and the total luminosity of the source above ~ 30 TeV. In order to disentangle better the influence of these different factors, we employ in this section a toy model: We use a uniform extragalactic magnetic field and a simple power-law as the energy spectrum of photons leaving a blazar.

If not otherwise specified, we use as reference parameters a uniform EGMF with field strength $B = 10^{-12}$ G, a power-law for the source energy spectrum of photons, $dN/dE \propto E^{-\gamma}$, with $\gamma = 2$, $E_{\text{max}} = 10^{17}$ eV and place our reference source at the distance of 135 Mpc, i.e. representative for Mrk 501.

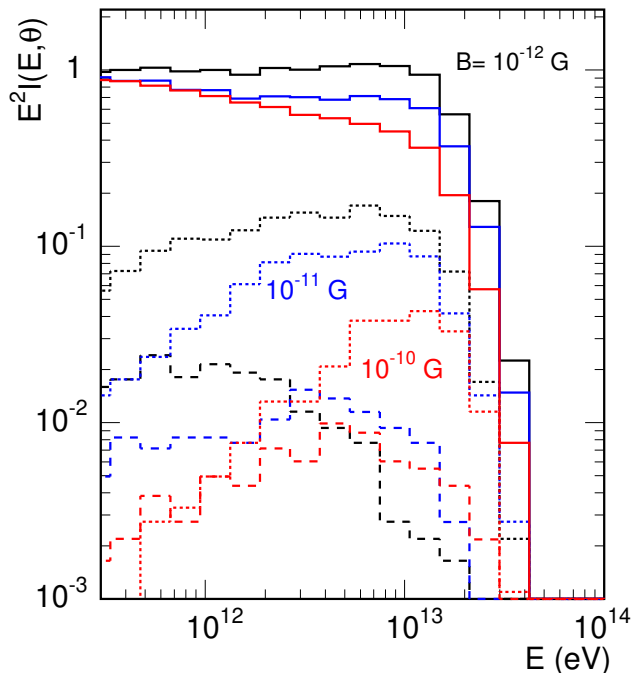


FIG. 2: The differential energy spectrum $I(E, \vartheta)$ for three different angular bins and a uniform magnetic field with strength $B = 10^{-12}$ G (black), 10^{-11} G (blue) and $B = 10^{-10}$ G (red).

a. Dependence on the EGMF strength We first discuss the change of the intensity profile $I(E, \vartheta) = d^2N(E, \vartheta)/d\Omega$ varying the strength of the EGMF. Figure 2 shows the differential energy spectrum $I(E, \vartheta)$ as function of the observed energy E for three ϑ bins: The curve labelled 'point' includes both the point-like and the halo component within $\vartheta < \vartheta_0 = 0.03^\circ$, while 'halo 1' denotes the mean intensity between $\vartheta_0 < \vartheta < 2\vartheta_0$ and 'halo 2' the intensity at $\vartheta = 0.6^\circ$. Our choice for the angular binning is related to the angular accuracy of present IACT (typically, few arcmin) and to experimental methodics of studying blazar halos: The intensity of γ -radiation from the angular vicinity of the source is compared to the background intensity in the field of view of the apparatus (typically, within 1 degree.). Thus, the feasibility of halo measurements can be characterized by the relative difference in the integral intensity between 'halo 1' and 'halo 2'. On the other hand, the overall sensitivity of an instrument to the halo component can be determined from the intensity ratio between the 'point-like' and 'halo 1' components. As the strength of the EGMF increases from $B = 10^{-12}$ G (left) to $B = 10^{-10}$ G (right), the $I(> E_0, \vartheta)$ distributions shown in Fig. 3 flatten, since the deflection angles increase. Moreover, the $I(> E_0, \vartheta)$ distributions for different E_0 become more similar to each other. As a result, the ratio between the halo intensity at small ϑ and the point-like intensity decreases too. As one can see from the figures, even for relatively strong magnetic fields with $B \sim 10^{-10}$ G a halo

observation is possible, in principle, if one restricts oneself with gamma energies in excess of 10 TeV. However, imposing such a cutoff would result in a drastic reduction of the observed flux, the measurement thus being hardly possible with present IACT sensitivity. Thus, the observation of blazar halos is more likely, if the line-of-sight to the blazar is contained in a void, where the fields of strength $B = 10^{-12}$ G may be typical.

b. Dependence on the spectral slope A comparison of the intensity profiles for two different values of the exponent, $\gamma = 2.0$ and 2.4 , in the power-law for the source energy spectrum of photons, $dN/dE \propto E^{-\gamma}$, is shown in Fig. 4. The halo component depends more weakly on the spectral slope γ than the point-like component, but its relative normalization decreases sharply for steeper source energy spectra. As a result, the ratio of halo and point flux decreases strongly towards lower energies. Nevertheless, the total number of halo events increases lowering the threshold energy E_0 . The optimal energy to look for the halo component depends also on the background of cosmic ray events and the background of point-like events with misreconstructed arrival direction. Therefore detailed studies taking into account the specific detector properties are required for such an optimization.

c. Dependence on the distance We compare the differential energy spectrum $I(E, \vartheta)$ of the point-like to the 'halo 1' and 'halo 2' components for two different distances in Fig. 5. If one factors out the trivial distance dependence, i.e. normalizes the flux at say 1 TeV to a constant value, then the halo components of sources at 135 and 300 Mpc show only minor differences: This behavior is explained by the fact that deflections at the distance l to the observer are weighted with the factor $\sim (L - l)/L$. Hence, deflections close to the observer contribute most to the size of the halo, while interactions at large distances lead mainly to a reduction of the observed flux. Moreover, the strongest deflection in case of a uniform EGMF considered here comes from the propagation of the last electron in the e/m cascade, which has the smallest energy, hence, is most strongly deflected by the field.

d. Dependence on high-energy luminosity We use again a power-law $dN/dE \propto E^{-2}$, varying now the maximal energy E_{\max} from $E_{\max} = 10^{13}$, 3×10^{13} , 10^{14} to 10^{15} eV. In Fig. 6, the influence of the luminosity injected above the pair-production threshold on the halo intensity is clearly visible. While close to the threshold an increase of E_{\max} leads to a strong enhancement of the halo component, a further increase of E_{\max} beyond 10^{15} eV has much smaller influence of the halo intensity for the chosen $1/E^2$ spectrum.

e. Dependence on the jet opening angle α_{\max} Finally we discuss the influence on the halo intensity of an anisotropic emission of the high energy photons. Qualitatively, one expects from Fig. 1, that restricting α to smaller and smaller values for a given ϑ requires that the last interaction at P happens closer and closer to the ob-

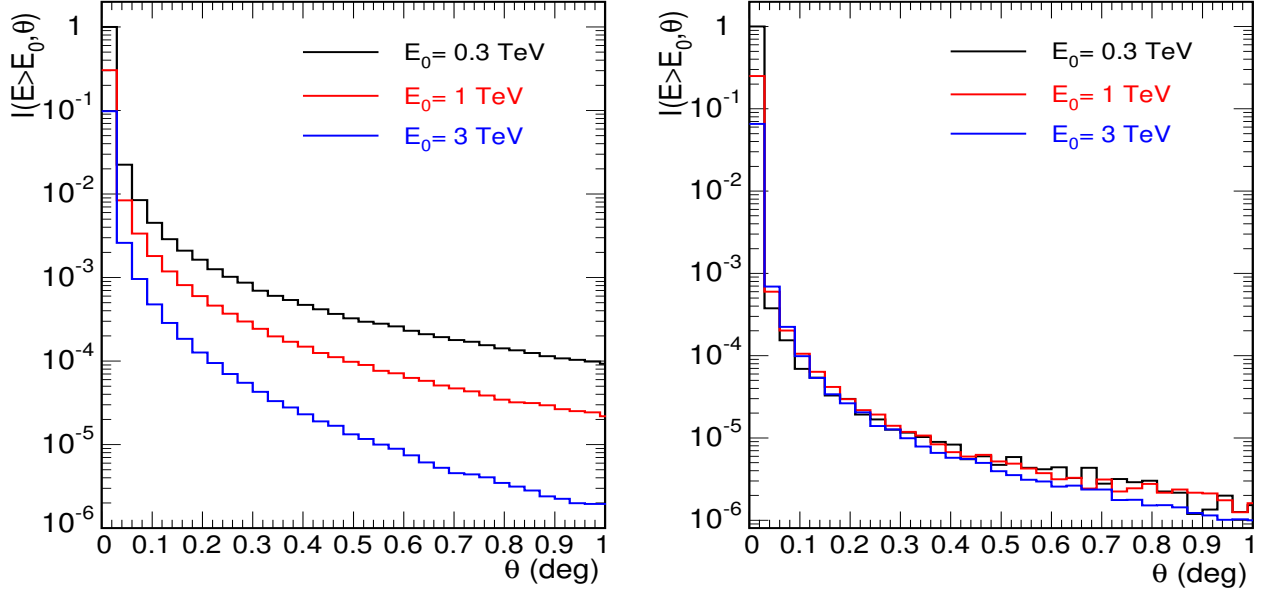


FIG. 3: The integral intensity $I(> E_0, \vartheta)$ as function of the angular distance ϑ to the source for a uniform magnetic field with strength $B = 10^{-12}$ G (left) and $B = 10^{-10}$ G (right).

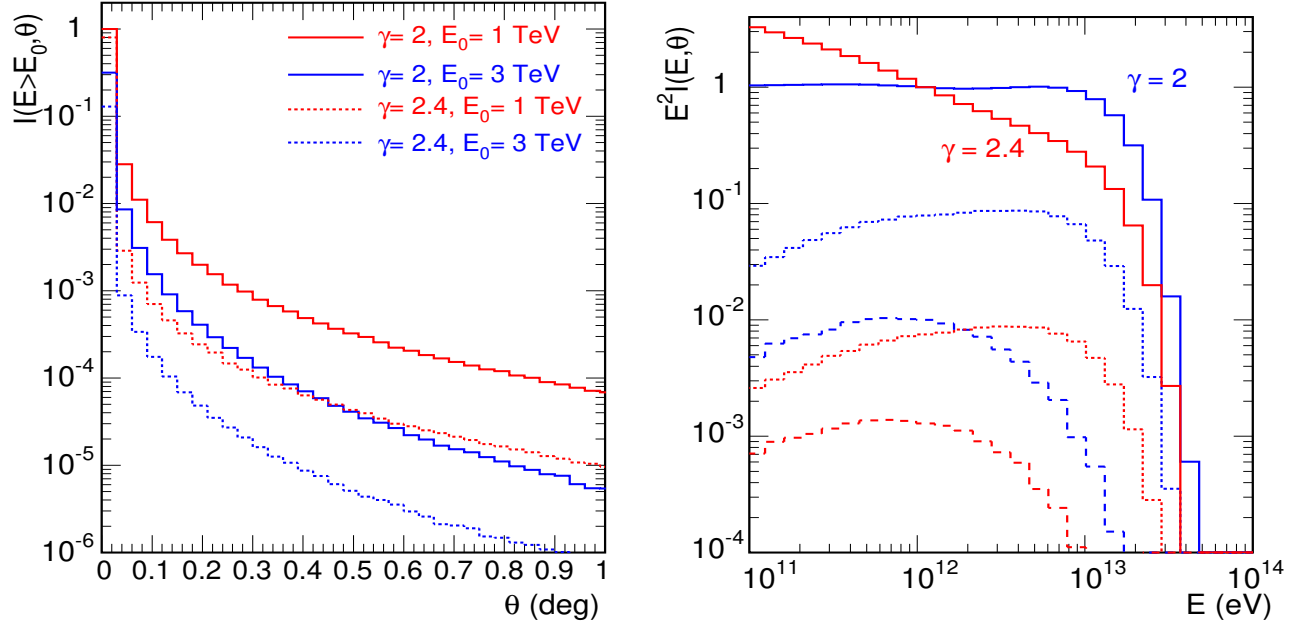


FIG. 4: Comparison of ϑ -dependence of integral intensity $I(> E_0, \vartheta)$ (left panel) and of differential energy spectra $I(E, \vartheta)$ (right panel) for different source spectra: power-laws with $\gamma = 2.0$ and $\gamma = 2.4$ (lower curves in the right panel; solid lines for point-like, dotted for 'halo 1', and dashed for 'halo 2'). A uniform magnetic field with strength $B = 10^{-11}$ G and the distance 134 Mpc is assumed.

server. Thus the intensity of the halo will be reduced on all angular scales, but we do not expect an angular cutoff as effect of an anisotropic emission by the source.

In order to obtain a quantitative understanding for the importance of beamed emission, we have recalculated our standard case restricting possible emission an-

gles α with respect to the line-of-sight to the blazar to $\alpha_{\text{jet}} = 60^\circ, 30^\circ, 15^\circ$ and 5° . The resulting integral intensity $I(\vartheta, > 300 \text{ GeV})$ as function of ϑ is shown in the right panel of Fig. 7, while we show the differential energy spectrum $I(E, \vartheta)$ of the point-like to the 'halo 1' and 'halo 2' components in the right panel. The integral intensity

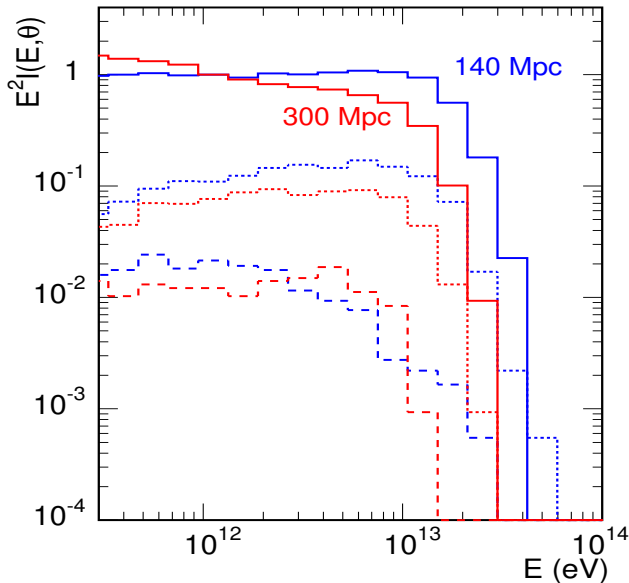


FIG. 5: Comparison of differential energy spectra for three angular bins for 140 and 300 Mpc source distance.

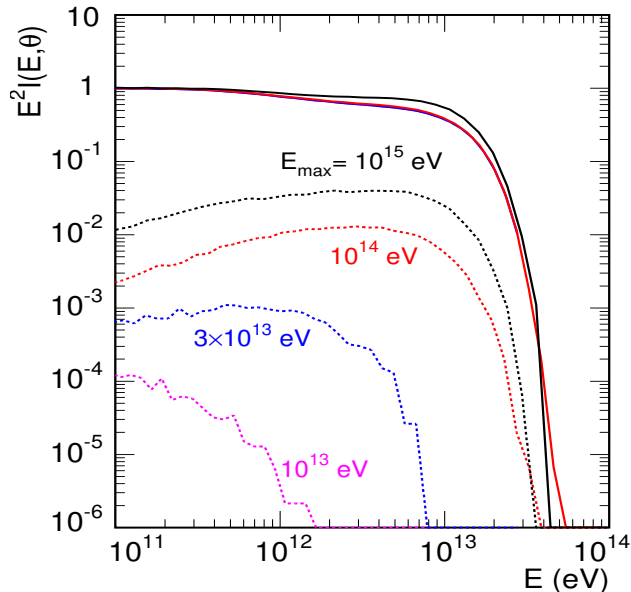


FIG. 6: Comparison of the differential energy spectra for the point-like and “halo 1” component, with three different energy cutoffs of the source spectrum: from top to down $E_{\text{max}} = 10^{15}, 10^{14}, 3 \times 10^{13}$ and 10^{13} eV.

$I(\vartheta, > 300\text{GeV})$ shows clearly an overall suppression as function of ϑ instead of a cutoff. The extent of this suppression becomes smaller at higher energies, but clearly the detection of blazar halos would disfavour the emission of the high energy component in a very narrow cone, $\alpha_{\text{jet}} \lesssim 10^\circ$.

In summary, we have found that the shape of the halo depends sensitively on all investigated parameters, but generally $I(E, \vartheta)$ decreases faster than the $1/\vartheta$ behavior suggested in Ref. [4]. The obtained enhancement of the small ϑ region, compared to Ref. [4], is due to the precise MC description of the cascade process, being related to the contributions from the tails of the distribution of the electron’s interaction length and of the secondary photon energies in ICS: Shorter distances travelled by electrons and higher energy of the parent electron producing the final photon result in smaller than average values of ϑ . Similarly, decreasing the opening ang of the high energy emission of photons in the source does not produce an angular cutoff in the observed photon spectrum, contrary to what has been suggested by the authors of Ref. [4]. The latter was an artifact of considering only the first two interaction steps in the electromagnetic cascade in Ref. [4]. Most importantly, we found that the intensity of the halo can exceed 1% of the point-like contribution at energies in excess of few TeV for field strengths $B = 10^{-12}$ G.

IV. HALO PREDICTIONS FOR SELECTED BLAZARS

We now turn from the toy model studied in the last section to a realistic study of the blazar halos for the five nearest blazars. The table I summarizes the distance, the observed (γ) and intrinsic (γ_s) spectral index assuming a power-law, the energy of the observed cut-off or the energy of the last measured data point as well as the reference used. As far as possible we used the photon spectra measured during quiet periods. While in the case of Mrk 421 the maximal energy $E_{\text{max}} = 1.4\text{TeV}$ corresponds to an observed cutoff in the measured energy spectrum, the numerical value of E_{max} corresponds otherwise to the last data point given in the cited references. From our discussion of the toy model, it is clear that the low luminosity of Mrk 421 above the pair creation threshold makes it an unfavorable candidate for the search of blazar halo. Therefore we will restrict our analysis to the remaining four blazars, Mrk 180, Mrk 501, 1ES 1959+650 and 1ES 2344+514.

We used the EGMF along the line-of-sight towards the four blazars that results from a constrained realization of the local universe (see Ref. [5] and references therein). In short, the initial density fluctuations were constructed from the IRAS 1.2-Jy galaxy survey by smoothing the observed galaxy density field on a scale of 7Mpc, evolving it linearly back in time, and then using it as a Gaussian constraint (see [18]) for an otherwise random realization of the Λ CDM cosmology. The volume constrained by the IRAS observations covers a sphere of radius ≈ 115 Mpc centered on the Milky Way and therefore encloses the prominent local structure including a fair representation of the large scale density field. Many of the most prominent clusters observed locally can therefore be identified

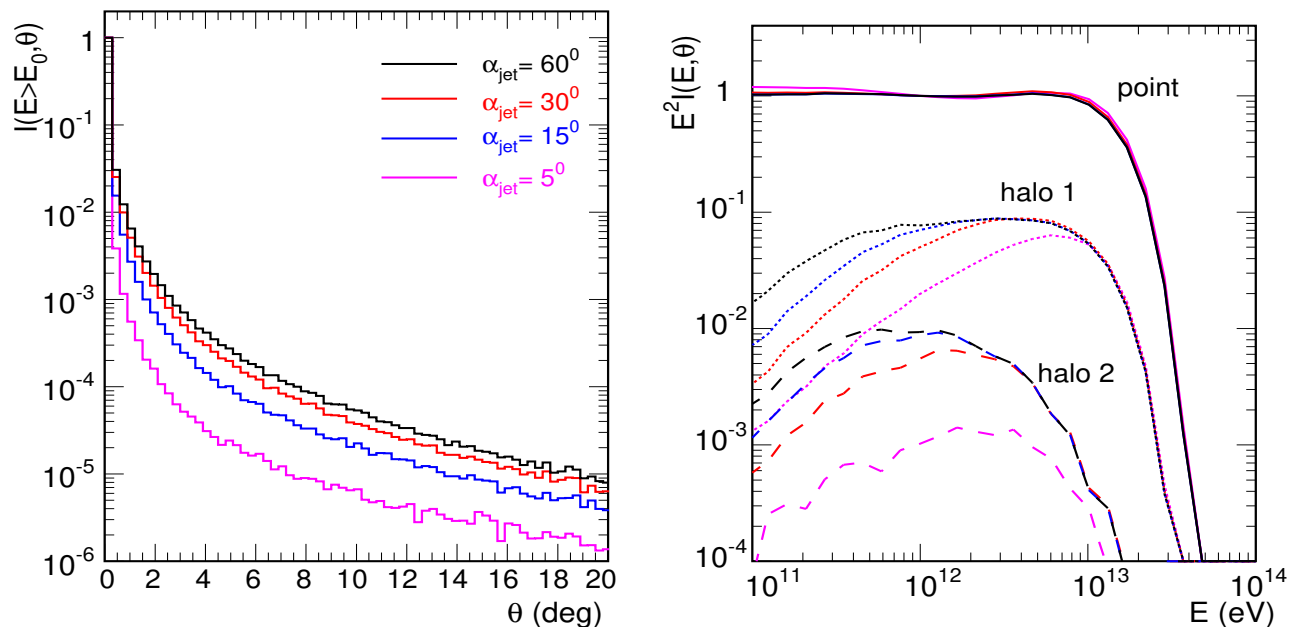


FIG. 7: Comparison of the differential energy spectra $I(E, \vartheta)$ (left panel) and of the ϑ -dependence of the integral intensity $I(> E_0, \vartheta)$ (right panel) for four different jet opening angles, $\alpha_{\text{jet}} = 60^\circ, 30^\circ, 15^\circ$ and 5° (from top to down).

directly with halos in the simulation, and their positions and masses agree well with their simulated counterparts (see also [19]). Although the smoothing of the observed galaxy density field when producing the initial conditions invokes spacial uncertainties within the simulated structures up to the used smoothing scale of 7 Mpc, the statistics of crossing filaments and voids within the local universe should nevertheless be quite realistic. This is especially the case for the objects considered in this study as we can make use of the full path length through the simulated volume as these objects are lying outside the simulated region.

For this work we used the magnetic field configuration obtained from two realizations (MHDy and MHDz) starting from different initial seed fields (for more details see Ref. [5]) having lower (MHDy) and higher (MHDz) initial values for the magnetic seed field. Both simulations lead to magnetic fields within the galaxy clusters which are statistically in agreement with the still rare Faraday rotation measures and are roughly bracketing the allowed range of magnetic fields in galaxy clusters.

A large fraction of the line-of-sight towards the blazars of interest are within the volume covered by this simulation, however it can cover only up to distances of ≈ 115 Mpc and we are forced to extend the magnetic field profile beyond that point. Since it is most important to reproduce the local field structure, we expect that the details of the chosen extension have only a minor influence as long the extended field has the correct statistical properties. In practise, we mirrored the field at the point of maximal distance along the line-of-sight. A comparison of the EGMF component perpendicular to the line-of-

sight towards Mrk 180 obtained in the models is shown in Fig. 10.

We will first present results for the model MHDz that generally predicts stronger localisation of magnetic fields in cluster and filaments and thus smaller deflections than model MHDy. A comparison of the field perpendicular to the line-of-sight towards Mrk 180 is shown for the two simulations in Fig. 10. Later, we compare the differences between our results for the two models.

We show our results¹ in Fig. 8 for Mrk 180 (top) and Mrk 501 (bottom) and in Fig. 9 for 1ES 1959+650 (top) and 1ES 2344+514 (bottom). The differential energy spectrum of each source is calculated for two different injection spectra: In the first case, we assume that the observed spectrum extends with the same slope γ_1 up to $E_{\text{max}} = 10^{17}$ eV. In the second case, we add a new, harder component with $\gamma_2 < \gamma_1$ that may be generated in particular by hadrons. Thus, we use as injection spectrum a broken power-law, adjusting the parameters like the break energy E_b such that we reproduce the observed spectral shape while optimizing the halo flux.

A characteristic feature of the second case is a small bump between the break energy and the exponential cut-off at E_{th} introduced by the EBL interactions. Clearly, blazars which show a cutoff at energies below E_{EBL} can have only a minor additional hard component compared to blazars which show either no cutoff or even a turn up.

¹ Numerical tables of these results can be obtained from MK.

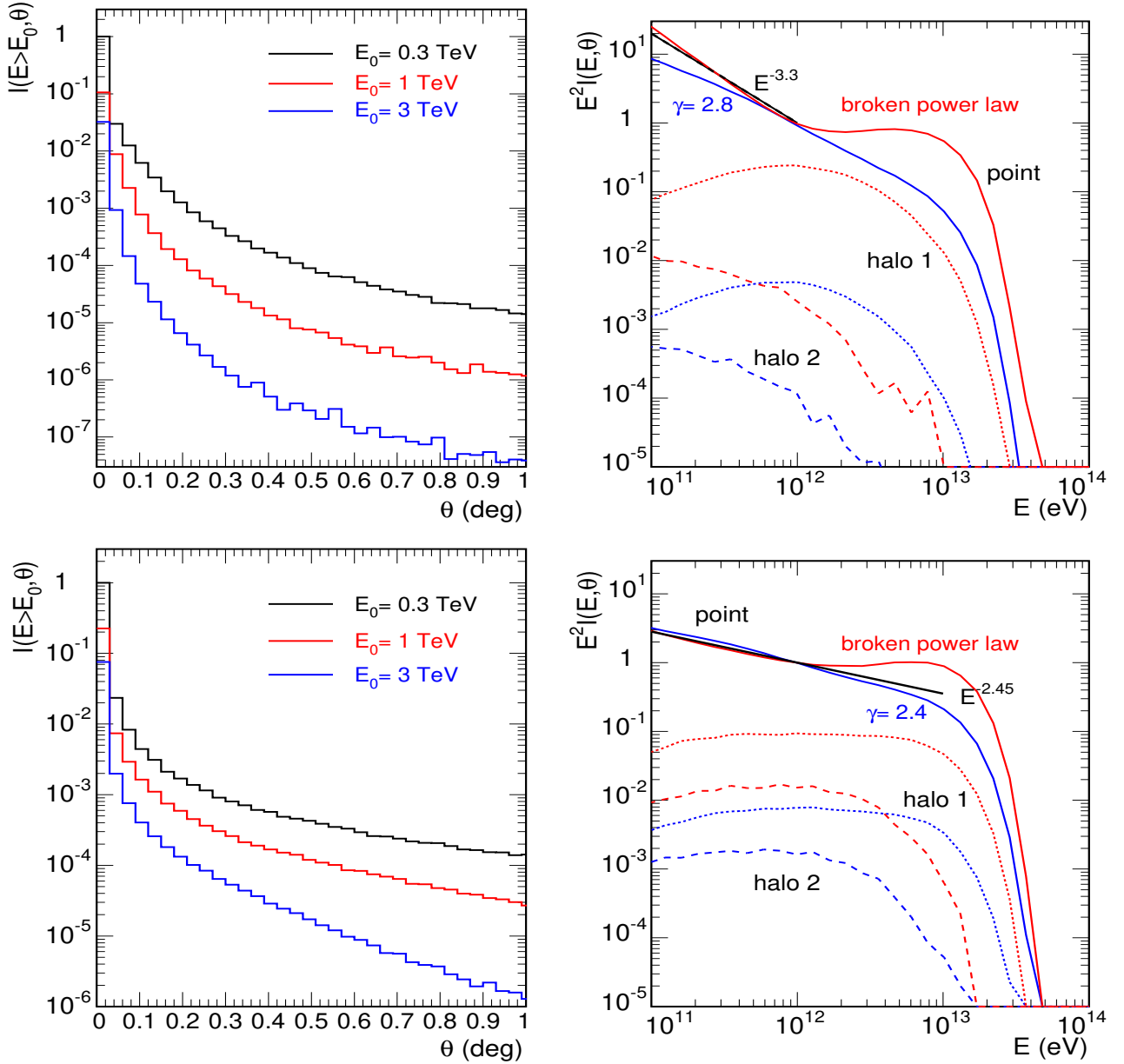


FIG. 8: Top: Mrk 180 (left panel: ϑ -dependence of integral intensity for the “broken” power-law initial spectrum with $\gamma_1 = 3.5$, $\gamma = 1.8$ and $E_b = 2$ TeV; right panel: differential energy spectra for three angular bins for the power-law source spectrum with $\gamma = 2.8$ and for the “broken” power-law case), bottom: Mrk 501 (left panel: ϑ -dependence of integral intensity for the “broken” power-law initial spectrum with $\gamma_1 = 2.4$, $\gamma = 2.0$ and $E_b = 5$ TeV; right panel: differential energy spectra for three angular bins for the power-law source spectrum with $\gamma = 2.4$ and for the “broken” power-law case); for all cases $E_{\max} = 10^{17}$ eV.

As one can see from the Figures, for the “broken” power-law case we get very pronounced halos in the TeV range for Mrk 180 and 1ES 2344+514, with the halo intensity being comparable to the one of the point-like component.

In Fig. 11, we compare the energy spectrum of Mrk 180 (left) and 1ES 2344+514 (right) obtained using the EGMF models MHDy and MHDz together with the “broken” power-law initial spectra. For both sources, we obtain a reduction of both point-like and halo intensities for

the MHDy realization of EGMF which is characterized by stronger and less localized magnetic fields. As one can see from Fig. 10, the strength of the perpendicular component of EGMF in the MHDy realization is almost an order of magnitude higher than in the MHDz case. This results in a reduction of the halo component for both sources considered, especially at lower energies. Nevertheless, for both realizations of the magnetic field structure, Mrk 180 and 1ES 2344+514 remain very promising

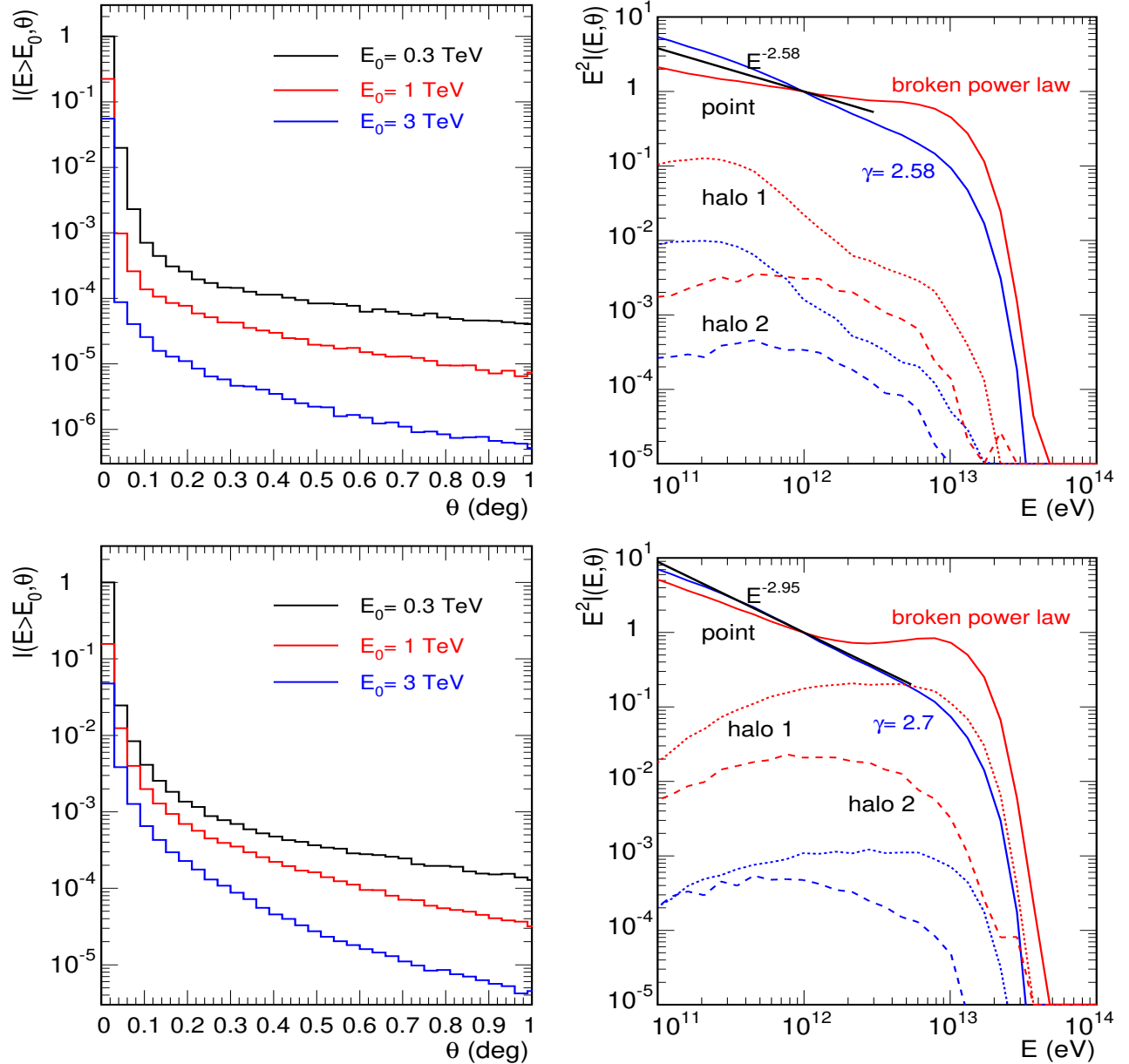


FIG. 9: top: 1ES1959+650, (left panel: ϑ -dependence of integral intensity for the “broken” power-law initial spectrum with $\gamma_1 = 2.6$, $\gamma = 1.8$ and $E_b = 3$ TeV; right panel: differential energy spectra for three angular bins for the power-law source spectrum with $\gamma = 2.58$ and for the “broken” power-law case), bottom: 1ES2344+514 (left panel: ϑ -dependence of integral intensity for the “broken” power-law initial spectrum with $\gamma_1 = 2.7$, $\gamma = 1.7$ and $E_b = 5$ TeV; right panel: differential energy spectra for three angular bins for the power-law source spectrum with $\gamma = 2.7$ and for the “broken” power-law case).

cases for the experimental detection of the halo in the TeV energy range.

Finally we note that the HEGRA experiment derived an upper limit of 1% on the halo flux from Mrk 521 at 0.5° during a burst period [17].

V. CONCLUSIONS

We have studied blazar halos generated by deflections of the charged component of electromagnetic pair cascades. The intensity of these halos depends mainly on the strength and the structure of the EGMF. Another necessary condition is the extension of the source energy spectrum above few $\times 10^{13}$ eV. Such a high energy extension of the source spectrum may be generated by high

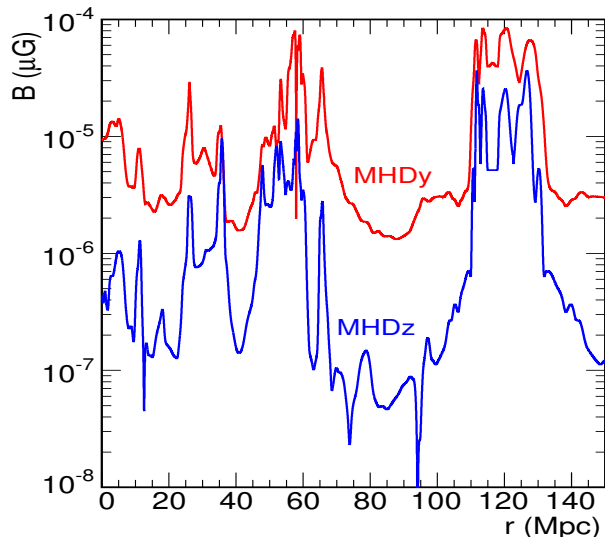


FIG. 10: The magnetic field B_{\perp} perpendicular to the line-of-sight towards Mrk 180.

Source	d_L/Mpc	γ	γ_s	$E_{\text{max}}/\text{TeV}$	Ref.
Mrk 421	130	2.2	2.2	1.4	[10]
Mrk 501	132	2.45	-	10	[11]
1ES 2344+514	183	2.95	2.66	5.4	[12]
Mrk 180	194	3.3	2.8	1	[13]
1ES 1959+650	198	2.58	-	3	[14, 15, 16]

TABLE I: List of considered blazars.

energy protons interacting with background photons in the source or emitting synchrotron or curvature radiation.

On the other hand, we found that the halo intensity is strongly suppressed if the high energy component is emitted in a very narrow cone, $\alpha_{\text{jet}} \lesssim 10^\circ$. The obtained integral intensity $I(\vartheta, > 300\text{GeV})$ in that case shows clearly an overall suppression as function of the observation angle, without angular cutoff. The extent of this suppression becomes smaller at higher energies, but clearly the

detection of blazar halos would disfavour the 'beamed' character of high energy photon emission.

Our analysis has accounted both for the kinematics of the pair-production and Compton processes without approximations as well as for the local structure of the EGMF by using EGMF models found earlier in a constrained simulation of structure formation including MHD processes. Halos with detectable intensity require very weak EGMFs, comparable to those found in the MHDz simulations of Ref. [5]. The direction of the EGMF vector close to the observer constitutes an uncertainty that cannot be resolved by numerical simulations. If the line-of-sight of a specific source and the EGMF vector are aligned close to the observer, the effect of EGMFs will be reduced.

In the most optimistic cases, the halo component found reaches 10% of the point-like component and may be already detected or excluded by current IACTs. An observation of blazar halos would provide valuable information on the EGMF along the line-of-sight to the source and on the minimal luminosity emitted above the pair creation threshold.

Finally, we comment on the generation of halos not by the electromagnetic cascade in the extralactic space but close to the source. A calculation of the halo intensity from this alternative mechanism requires a detailed model for the photon backgrounds and the magnetic field in the source. Moreover, the model for acceleration, in particular the acceleration site, has to be specified. While it is thus clear that an additional contribution to the halo from processes close to the source exists, detailed predictions will be strongly model dependent.

Acknowledgments

We would like to thank Tanja Kneiske, Julian Sitarek and especially Dieter Horns for helpful comments and suggestions. S.O. acknowledges a Marie Curie IEF fellowship from the European Community, R.T. partial support from the Deutsche Forschungsgemeinschaft within the SFB 676.

-
- [1] W. Hofmann, J. Phys. Conf. Ser. **120**, 062005; D. Horns, arXiv:0808.3744 [astro-ph], to appear in Reviews of Modern Astronomy.
- [2] A. I. Nikishov, Sov. Phys. JETP **14**, 393 (1962).
- [3] F. A. Aharonian, P. S. Coppi and H. J. Volk, Astrophys. J. **423**, L5 (1994) [arXiv:astro-ph/9312045]. See also S. Gabici and F. A. Aharonian, Phys. Rev. Lett. **95**, 251102 (2005) [arXiv:astro-ph/0505462].
- [4] A. Neronov and D. V. Semikoz, JETP Lett. **85**, 473 (2007) [arXiv:astro-ph/0604607]; for a related work considering the FERMI energy range see K. Murase, K. Takahashi, S. Inoue, K. Ichiki and S. Nagataki, arXiv:0806.2829 [astro-ph], to appear in Atrophys. J. Lett.
- [5] K. Dolag, D. Grasso, V. Springel and I. Tkachev, JCAP **0501**, 009 (2005) [astro-ph/0410419].
- [6] M. Sikora and G. Madejski, AIP Conf. Proc. **558**, 275 (2001) [arXiv:astro-ph/0101382].
- [7] K. Mannheim, Astron. Astrophys. **269**, 67 (1993) [arXiv:astro-ph/9302006]; F. A. Aharonian, New Astron. **5**, 377 (2000) [arXiv:astro-ph/0003159]; A. Mücke and R. J. Protheroe, Astropart. Phys. **15**, 121 (2001) [arXiv:astro-ph/0004052]; M. Kachelrieß, S. Ostapchenko and R. Tomàs, arXiv:0805.2608 [astro-ph], to appear in New J. of Phys.
- [8] T. M. Kneiske, K. Mannheim and D. H. Hartmann, As-

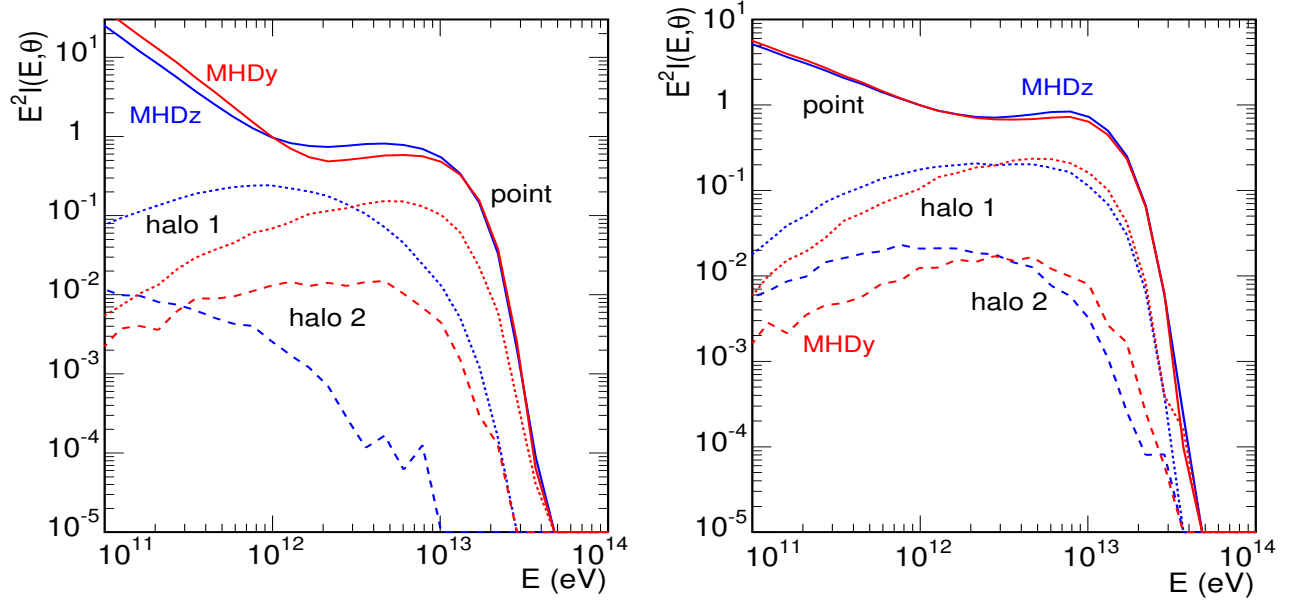


FIG. 11: Comparison of differential energy spectra for three angular bins for two realizations of EGMF (MHDy [red] and MHDz [blue]) for Mrk 180 (left panel) and for 1ES 2344+514 (right panel).

- tron. Astrophys. **386**, 1 (2002) [arXiv:astro-ph/0202104];
T. M. Kneiske, T. Bretz, K. Mannheim and D. H. Hartmann, Astron. Astrophys. **413**, 807 (2004) [arXiv:astro-ph/0309141].
[9] R. J. Protheroe and P. L. Biermann, Astropart. Phys. **6**, 45 (1996) [Erratum-ibid. **7**, 181 (1997)] [arXiv:astro-ph/9605119].
[10] J. Albert *et al.* [MAGIC Collaboration], Astrophys. J. **663**, 125 (2007) [arXiv:astro-ph/0603478].
[11] J. Albert *et al.*, Astrophys. J. **669**, 862 (2007) [arXiv:astro-ph/0702008].
[12] J. Albert *et al.* [MAGIC Collaboration], Astrophys. J. **662**, 892 (2007) [arXiv:astro-ph/0612383].
[13] J. Albert *et al.* [MAGIC Collaboration], Astrophys. J. **648**, 105 (2006) [arXiv:astro-ph/0606630].
[14] G. Tagliaferri *et al.*, Astrophys. J. **679**, 1029 (2008) [arXiv:0801.4029 [astro-ph]].
[15] E. Aliu *et al.* [MAGIC Collaboration], Astrophys. J. **639**, 761 (2006) [arXiv:astro-ph/0508543].
[16] F. Aharonian, A. Akhperjanian and M. Beilicke [HEGRA Collaboration], Astron. Astrophys. **406**, L9 (2003) [arXiv:astro-ph/0305275].
[17] F. A. Aharonian *et al.* [HEGRA Collaboration], arXiv:astro-ph/0012401.
[18] Y. Hoffman and E. Ribak, Astrophys. J. Lett. **380**, L5 (1991).
[19] H. Mathis *et al.*, MNRAS, **333**, 739 (2002).